J Solid State Electrochem (2011) 15:2667–2674
DOI 10.1007/s10008-010-1258-7

ORIGINAL PAPER

Preparation of activated carbon from polyaniline by zinc chloride activation as supercapacitor electrodes

Xiaoxia Xiang · Enhui Liu · Zhengzheng Huang · Haijie Shen · Yingying Tian · Chengyi Xiao · Jingjing Yang · Zhaohui Mao

Received: 5 August 2010 / Revised: 16 November 2010 / Accepted: 23 November 2010 / Published online: 8 December 2010

Abstract Activated carbon for supercapacitor electrode was prepared from polyaniline using chemical activation with $ZnCl_2$. The morphology, surface chemical composition, and surface area of the as-prepared carbon materials were investigated by scanning electron microscope, atomic force microscopy, X-ray photoelectron spectroscopy, and Brunauer–Emmett–Teller measurement, respectively. Electrochemical characteristics were evaluated by cyclic voltammograms, galvanostatic charge/discharge, and electrochemical impedance spectroscopy tests in 6.0 mol L^{-1} KOH aqueous solution. The electrochemical measurements showed that $ZnCl_2$ activation led to better capacitive performances. The activated carbon presented a high-specific gravimetric capacitance of 174 $F g^{-1}$, with rectangular cyclic voltammetry curves at a scan rate of 2 mV s^{-1}, and it remained 93% even at a high scan rate of 50 mV s^{-1}. These demonstrated that activated carbon would be a promising electrode material for supercapacitors.

Keywords Supercapacitor · Polyaniline · Activated carbon · X-ray photoelectron spectroscopy · Zinc chloride

Introduction

Supercapacitors (generally called electrochemical capacitors) have gained much attention in recent years because of their high power density, excellent reversibility, and long cycle life [1, 2]. On the basis of energy storage mechanisms, the supercapacitors are classified as electrical double-layer capacitors (EDLCs) and faradaic pseudocapacitors. In EDLCs, energy storage is accumulated from the electronic and ionic charges between electrode/electrolyte double-layer interfaces, while faradaic pseudocapacitors store energy by a fast and reversible faradaic redox reaction at or near the electrode surface [3–5].

As it is well known, electrode material is one of the dominating factors that influence the performance of supercapacitor. Among various electrode candidates for supercapacitors, activated carbons have attracted considerable interest owing to their high-specific surface area, highly porous structure, good electrical conductivity, and relatively low cost [6–8]. Because the choices of carbon precursor and activation conditions determine the electrochemical performance, with carbon surface area, pore size distribution, electrical conductivity all affecting double-layer capacitance. Supercapacitors with activated carbon electrodes derived from various precursors such as sawdust [7], cationic starch [9], bagasse [10], and coffee shell [11] have been reported.

Broadly, the preparation of activated carbon can be divided into physical activation and chemical activation. In physical activation, the raw material is carbonized under an inert atmosphere and then activated at high temperature by using an activating reagent such as steam [12] or carbon dioxide [4, 13]. In chemical activation, firstly, the precursor is mixed with some chemical reagents, such as $ZnCl_2$ [7, 9, 10, 14], KOH [2, 3, 15, 16], and H_3PO_4 [17–19]. Then it is carbonized and washed to get the final activated carbon. Generally, chemical activation is the preferred route because it achieves higher yield, larger surface area, needs low operating temperature, and is cost-effective [3].

In this paper, we have prepared activated carbon with good electrochemical performance from polyaniline (PANI)

X. Xiang · E. Liu (✉) · Z. Huang · H. Shen · Y. Tian · C. Xiao · J. Yang · Z. Mao
Key Laboratory of Environmentally Friendly Chemistry and Applications of Ministry of Education, College of Chemistry, Xiangtan University,
Hunan 411105, People's Republic of China
e-mail: liuenhui99@sina.com.cn

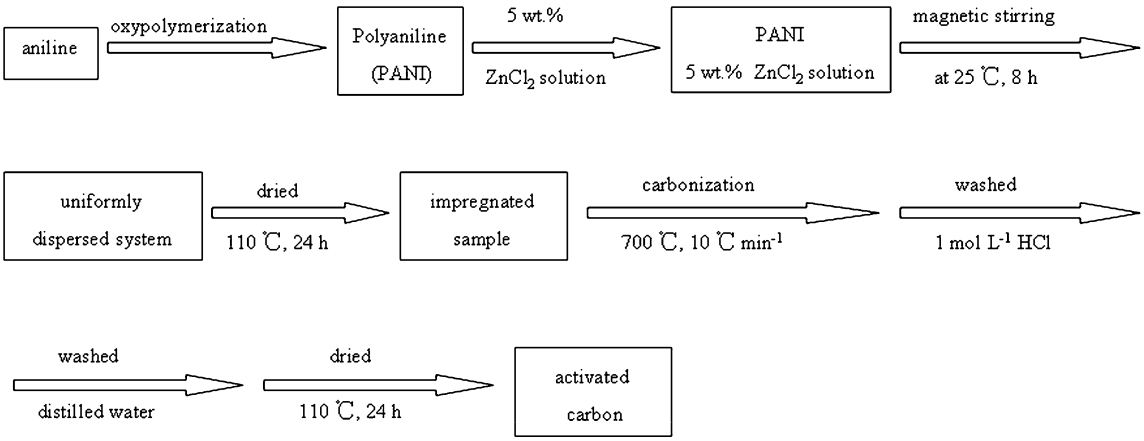

Fig. 1 Schematic illustration for preparing for activated carbon

through $ZnCl_2$ activation. PANI contains about 15% of nitrogen and 79% of carbon, and has the advantages of low cost, environmental stability, and easy to synthesize [20, 21]. Moreover, the amount of nitrogen introduced to the activated carbon is believed to be dependent on the nitrogen precursor [22]. In addition, nitrogen can enhance the specific capacitance by improved wettability of carbon surface and pseudocapacitance reactions [23]. For these reasons, we believe that PANI is a promising nitrogen-containing material as precursor to prepare activated carbon for supercapacitors. To the best of our knowledge, this is the first time to synthesize such an activated carbon material for supercapacitors in this way. Especially, the textural and electrochemical properties of the carbon materials are discussed in detail.

Experimental

Preparation of activation carbon materials

PANI was prepared by the oxypolymerization method which was reported by Liu et al. [20]. The PANI was mixed with a 5.0 wt.% $ZnCl_2$ solution under vigorous stirring for 8 h, and then it was dried at 110 °C for 24 h to prepare the impregnated sample. The weight ratio of PANI to $ZnCl_2$ was 1:1. For activation, the impregnated material was transferred into a graphite crucible and was heated at the rate of 10 °C min^{-1} from room temperature up to 700 °C under nitrogen flow. Then, it was cooled back to the initial temperature. The as-prepared product was subsequently washed with 1 mol L^{-1} HCl and distilled water until the pH of the solution was approximately 7. The final product was dried at 110 °C for 24 h under vacuum condition. The preparation strategy is shown in Fig. 1. The obtained activated carbon was marked as CZ. For comparison, a carbonized sample was prepared from PANI without $ZnCl_2$. The preparative procedure was the same as that of CZ, the sample was marked as CC.

The characterization of materials

Scanning electron microscope (SEM) measurements were performed on a JSM-6610LV scanning electron micro-

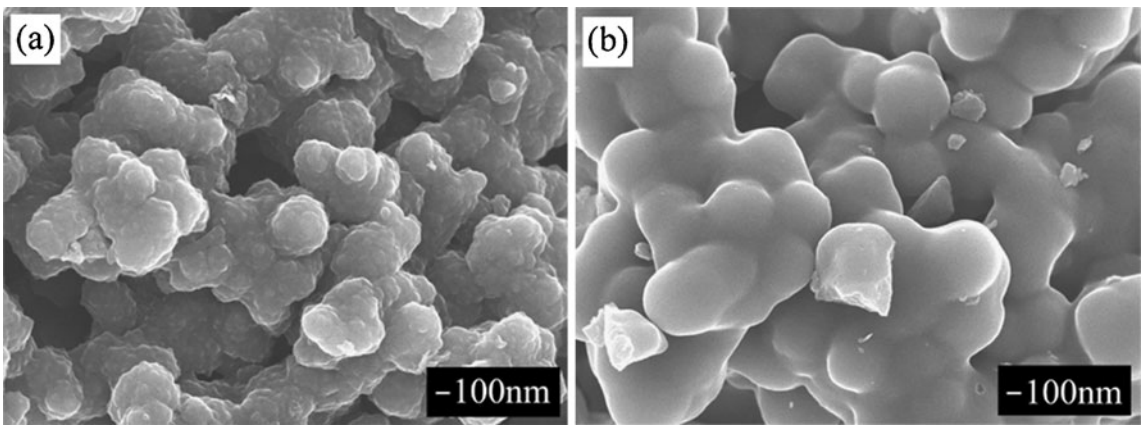

Fig. 2 SEM images of **a** CC and **b** CZ

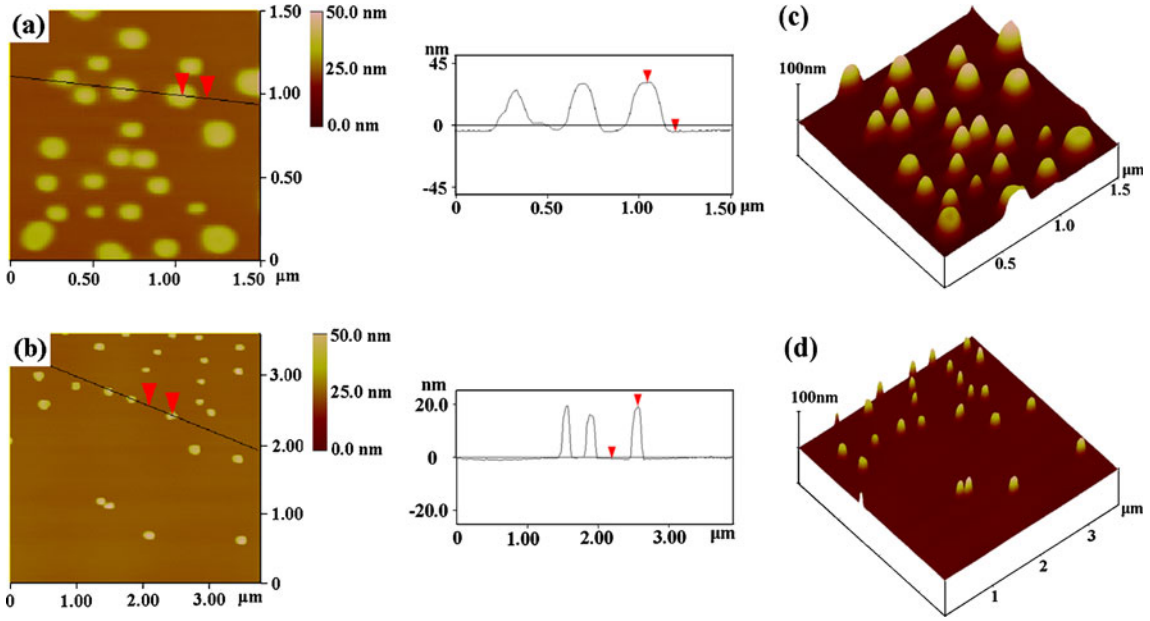

Fig. 3 Two-dimensional AFM images and corresponding cross-section of CC (**a**) and CZ (**b**). Three-dimensional AFM images of the CC (**c**) and CZ (**d**)

scope. Atomic force microscopy (AFM) imaging of prepared diatoms was performed using a Multimode NS3D (Veeco Corp, USA). Images were acquired in air using contact modes. The Brunauer–Emmett–Teller (BET) specific surface area and pore volumes of the carbon materials were determined by N_2 adsorption at 77 K on a Quantachrome NOVA-2200 system. The elemental analyses were performed on an elemental analyzer Vario EL V5 (Elementar Analysensysteme GmbH). The chemical state of the surface was characterized by X-ray photoelectron spectroscopy (XPS) on a VG Scientific ESCALAB 250 spectrometer with an Al Kα source. The spectra were charge corrected using the C1s peak (Eb (C1s)=284.6 eV) as an internal standard. A non-linear, Shirley-type baseline and an iterative least-squares fitting algorithm were used to decompose the peaks, the curves being taken as 80% Gaussian and 20% Lorenzian. The surface atomic ratios were calculated from the ratio of the corresponding peak areas after correction with the theoretical sensitivity factors based on the Scofield's photoionization cross-sections.

Electrochemical test

The electrode was consist of 80% as-prepared carbon material, 10% acetylene black (AB) as conducting agent, and 10% polyvinylidene fluoride (PVDF) as a binder. First, PVDF was dissolved in N-methyl-2-pyrrolidone, AB and carbon material were mixed orderly to form a homogeneous slurry, which was subsequently blush-coated onto nickel foam current collectors (Φ=10 mm). Then, the electrodes were dried in a vacuum oven at 110 °C overnight. Sandwich-type capacitors were assembled with two electrodes separated by nylon film, and 6 mol L^{-1} KOH solution was used as electrolyte. Cyclic voltammetry (CV), galvanostatic charge/discharge cycles, and electrochemical impedance spectroscopy (EIS) were conducted on a CHI 660A electrochemical workstation (CHI Inc., USA) at room temperature. EIS measurements were carried out by applying an AC voltage of 5 mV amplitude in the 100 kHz to 10 mHz frequency range.

The specific capacitance of the electrode is obtained from the Eq. (1):

$$C_g = \frac{I\Delta t}{m\Delta V} \times 2 \quad (1)$$

Where C_g is the specific gravimetric capacitance (F g^{-1}), I is the current loaded, Δt is the discharge time (s), ΔV is the potential change during the discharge process (1 V in this study), and m (g) represents the mass of the activated carbon.

Table 1 Textural characteristics and specific capacitance of the CC and CZ

Samples	Surface area (m^2 g^{-1})	Pore volume (cm^3 g^{-1})	Pore diameter (nm)	C_{spec} (F g^{-1})
CC	13.8	0.022	1.68	12
CZ	824	0.210	1.43	174

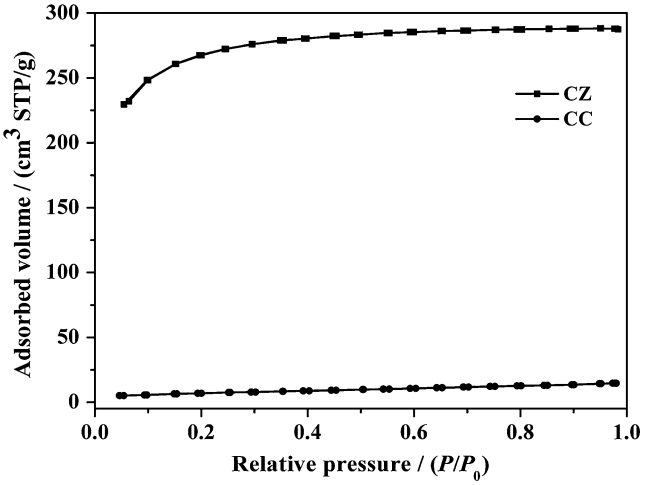

Fig. 4 N_2 adsorption/desorption isotherms of the CC and CZ

Results and discussion

Characteristics of the carbon samples

Figure 2a depicts representative SEM photograph of the CC. It is granular, and a lot of granular which are in similitude size stack together. The morphology of CZ is similar to CC (Fig. 2b), however, its surface is quite smooth. The reasons may be the breakage of some chemical bonds and partial oxidation of carbon surface. Accordingly, distinction in the surface morphology would lead to distinction in the specific gravimetric capacitance.

Atomic force microscopy was performed to examine the surface morphology and to measure roughness values for CC and CZ. Typical two- and three-dimensional AFM images with corresponding cross-section graphs of CC and CZ are shown in Fig. 3. As can be seen, some isolated particles at a density lower than 11 and 2 particles μm^{-2} appear on the surface for CC and CZ, respectively. It also can be observed from the AFM images that CC contains many large particles and exhibits an uneven distribution of particle sizes. However, after activation, as for the CZ, uniform and small particles are observed. In addition, the average heights of particles are 32 and 20 nm for CC and CZ, respectively. These may be the reasons for the enhancement of surface area (see Table 1). The cross-section of each AFM image is analyzed in terms of surface average roughness. The CZ surface has a root mean square roughness (rms) 7.298 nm (measured on 3×3 μm area), while the CC has an rms roughness of 14.660 nm (measured 1.5×1.5 μm area). These results confirm the lower surface roughness of CZ in comparison with CC, confirms the SEM observations.

Typical nitrogen adsorption/desorption isotherms of the CC and CZ are shown in Fig. 4. In the isotherm of CC, the adsorbed volume is very small, indicating its nonporous characteristics. According to the IUPAC classification, the N_2 adsorption isotherm of CZ exhibits type I characteristics, indicating its microporous features.

Table 1 summarizes the textural properties of the samples. It is clear that both the specific surface area and total pore volume of CC are less than those of CZ. CC possesses very low surface area (13.8 $m^2\ g^{-1}$) because of its nonporous characteristics. However, the surface area of CZ is sharply increased through $ZnCl_2$ activation, and the value is as high as 824 $m^2\ g^{-1}$. For the sample CZ, the $ZnCl_2$ is assumed a dehydration agent during activation. It inhibits the formation of tars and any other liquids that can clog up the pores of the sample, and volatiles will be subsequently released from the carbon surface [24]. The specific gravimetric capacitance is also shown in Table 1. It can be observed that CZ with the high BET surface area has the high-specific gravimetric capacitance of 174 Fg^{-1}. This means that the enhanced capacitance can be mainly attributed to the enhancement of the surface area.

Owing to the fact that XPS determines the surface composition in contrary to bulk composition revealed by elemental analysis, the relative contents of surface carbon, oxygen, and nitrogen obtained from XPS differed from those from elemental analyzes (Table 2). More surface oxygen and less surface nitrogen are measured in CZ than in CC, which is in agreement with the results of elemental analysis.

XPS spectra of investigated carbon materials indicate the presence of three distinct peaks due to carbon, nitrogen, and oxygen in Fig. 5. The binding energies corresponding to appropriate peaks are as follows [23, 25–28]:

C1s: (1) 284.5±0.1 eV, graphitic carbon (C=C), and C–H groups; (2) 286.1±0.1 eV, phenolic, alcohol, and ether (C–O) or C–N groups; (3) 287.4±0.2 eV, carbonyl or quinone groups (C=O); (4) 289.3±0.1 eV, carboxyl groups (COO^-); (5) 291.6±0.4 eV π-π* transitions in aromatics.

Table 2 Carbon, hydrogen, oxygen, and nitrogen contents [%] in the studies samples obtained from elemental analyses and X-ray photoelectron spectroscopy (hydrogen is not included)

Samples	C	H	N	O	C_{XPS}	O_{XPS}	N_{XPS}	N/C
CC	80.4	1.69	9.76	8.15	73.4	10.2	16.4	0.22
CZ	68.4	1.78	7.91	21.9	70.4	16.3	13.3	0.19

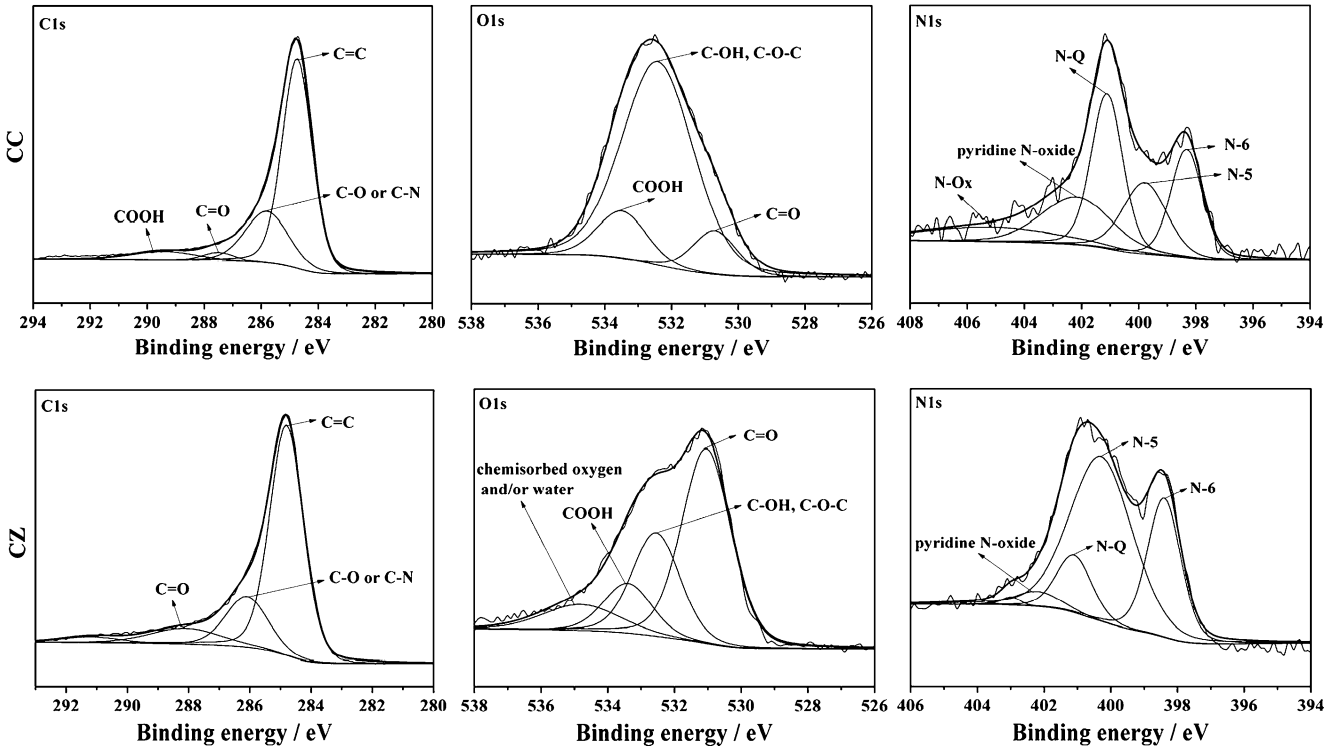

Fig. 5 X-ray photoelectron spectra of the CC and CZ

N1s: (1) 398.7±0.3 eV, pyridinic (N-6); (2) 400.5±0.3 eV, pyrrolic and pyridonic (N-5); (3) 401.3±0.3 eV, quaternary nitrogen (N-Q); (4) 402.8±0.4 eV, pyridine N-oxide; (5) 404–406 eV, chemisorbed nitrogen oxides (N-Ox).

O1s: (1) 531.3±0.2 eV, carbonyl (C=O) and/or quinone (marked as O-I); (2) 532.6±0.3 eV, hydroxyl (C–OH) and ether (C–O–C) (marked as O-II); (3) 534.3±0.2 eV, carboxyl (COO^{-}) (marked as O-III); (4) 536.3±0.4 eV, chemisorbed oxygen and/or water.

As seen from Table 3 and Fig. 5, compared with the sample CC, CZ from $ZnCl_2$ activation leads to an increase in the concentration of surface oxygen functional groups and a change in their distribution. The content of carbonyl and/or quinone group of CZ increases relatively at the expense of C-OH and/or C-O-C groups. Rufford et al. [10] have proved that $ZnCl_2$ activation had a large effect on the oxygen and nitrogen functional groups.

The types of nitrogen species and their distribution are shown in Table 3. The activated sample CZ has a much lower content of nitrogen than CC. Jurewicz et al. [29] have mentioned that activation of the nitrogen enriched precursor led to a reduction of the nitrogen content but also to the conversion of the surface nitrogen species. To understand the role of nitrogen functionalities in capacitive performance, it is necessary to clarify the types of nitrogen introduced onto the carbon surface. The locations of nitrogen functionalities within the carbon matrix are schematically displayed in Fig. 6. The peak analyses of N1s for CZ and CC reveal the nitrogen species are almost the same, but with different relative contributions. The content of pyridinic nitrogen after activation increases to 26.2%. Similarly, the content of N-5 nitrogen in CZ is about three times higher than that in CC. A small amount (12%) of N-Ox groups is found in CC. The increase of N-5 is probably caused by by transformation of other nitrogen species during activation processing (e.g., N-Ox groups) to more thermally stable nitrogen species [25]. It is reported that the most important functional groups affecting energy storage performance are pyrrolic and pyridinic nitrogen along with quinone oxygen [28, 30].

Table 3 Relative surface concentrations of nitrogen and oxygen species obtained by fitting the N1s and O1s core level XPS spectra

Samples	N-6 398.7 eV	N-5 400.5 eV	N-Q 401.3 eV	N-X 402.8 eV	N-Ox 405 eV	O-I 531.3 eV	O-II 532.6 eV	O-III 534.3 eV
CC	20.5	18.5	29.2	19.8	12.0	10.4	77.2	12.4
CZ	26.2	57.6	11.5	4.7	–	50.9	26.0	12.7

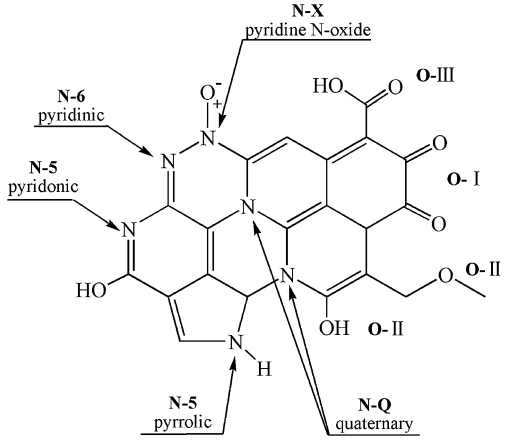

Fig. 6 Schematic diagram of nitrogen- and oxygen-containing surface functional groups on carbon

Electrochemical properties

Typical CV curves for CZ and CC at a scan rate of 2 mV s^{-1} are presented in Fig. 7a. The CV curve of CZ exhibits larger area of rectangle than that of CC, suggesting CZ has higher specific capacitance. The CC sample shows irregular rectangular shape and it gives a capacitance of 12 $F g^{-1}$. The irregular rectangle may be due to diffusion-limited capacitance, which may in turn be due to electrolyte tapped in the micropores of the carbon [11]. Figure 7b presents the CV curves for sample CZ at various scan rates changing from 2 to 50 mV s^{-1}. At 2, 5, and 10 mV s^{-1}, the curves present a standard quasi-rectangular voltammogram shape. At increase scan rate of 50 mV s^{-1}, the rectangular shape of votammogram of CZ is maintained with only slight distortion. As the scan rate increases from 2 to 50 mV s^{-1}, the specific gravimetric capacitance of CZ only decrease from 174 to 161 $F g^{-1}$ with a retain ratio of 93%. The good electrochemical performance of the CZ can be attributed to the presence of the pyridinic and pyrrolic nitrogen along with quinone oxygen, in which almost 84% of the nitrogen functionalities are pyridinic and pyrrolic. Pandolfo et al. [8] also have mentioned that functional groups could enhance the wettability of carbon electrodes and, consequently, increase the specific capacitance of the carbon through improved pore access and greater surface utilization.

Galvanostatic charge/discharge measurements are commonly used to test the performance of capacitors. Figure 8a displays the galvanostatic charge/discharge curves of the CC and CZ at the current density of 500 mA g^{-1}. It can be seen that the CZ exhibits almost the isosceles triangle curve, which indicate the supercapacitor with the performance of reversibility and good capacitive. The specific capacitance of CZ reaches 166 $F g^{-1}$, much larger than that of the CC (7 $F g^{-1}$). The better electrochemical performance of the CZ can be ascribed to its higher surface area and micropore volume. The abundant micropores play an essential role for optimizing the electrical double-layer surfaces and then strengthen the value of capacitance. In addition, the result suggests that, after activation more surface area of the carbon is accessible to electrolyte ions due to the improved wettability of carbon and more quick charge propagation [31]. Figure 8b shows the galvanostic charge/discharge curve of CZ at different current densities. The specific gravimetric capacitance drops slowly as the current density increases. This indicates that the ions have enough time to diffuse into the micropores of carbons at the low current density, while the ions can only partially penetrate into the micropores due to the sterical limitations at the high current density [8, 16]. Although the specific capacitance depressed, it can still remain as high as 140 F g^{-1} at a higher current density of 5 $A g^{-1}$. The good performance of CZ demonstrates that PANI activated carbon will be a promising electrode material for supercapacitors.

Figure 9 shows the cyclic stability of CZ electrodes at the current density of 500 mA g^{-1}. During the initial cycles,

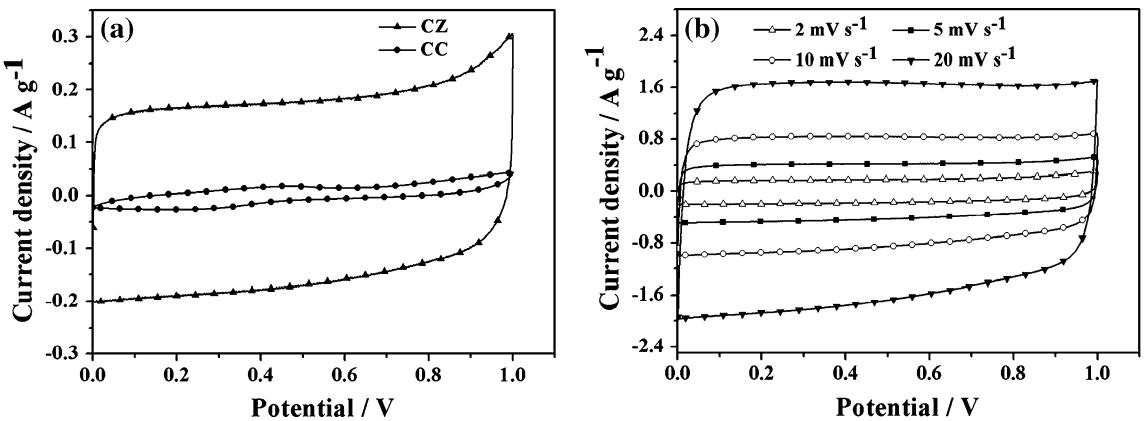

Fig. 7 Cyclic voltammograms of carbon electrodes in 6 mol L^{-1} KOH electrolyte, **a** the CC and CZ at a scan rate of 2 mV s^{-1}, **b** the CZ with different scan rates

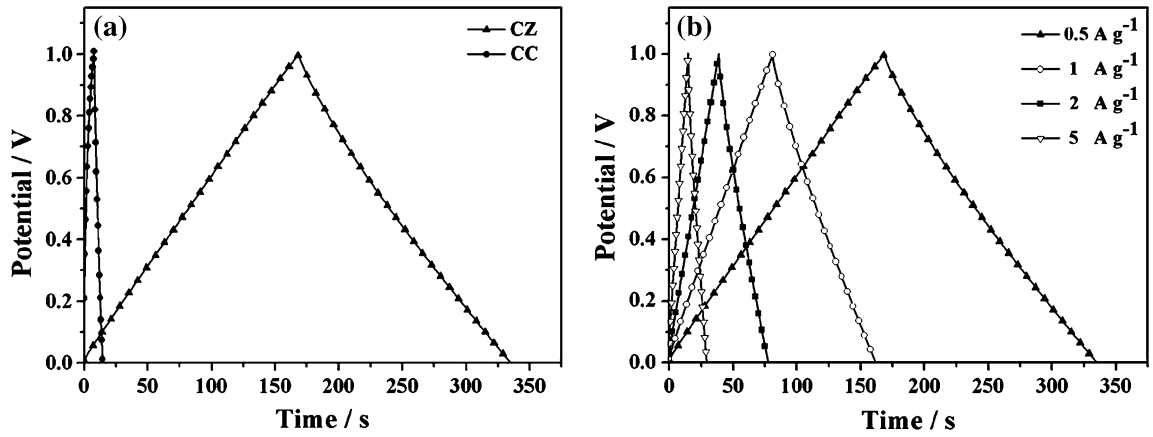

Fig. 8 Galvanostatic charge/discharge curves of carbon electrodes in 6 mol L^{-1} KOH electrolyte, **a** the CC and CZ at the current density of 500 mA g^{-1}, **b** the CZ performed at different current density

it is found that there is a gradual increase in the specific capacitance value from 166 to 171 Fg^{-1} in the first 400 cycles, which was due to electrochemical activation. A little decrease is observed from 400 to 1,000 cycles, and thereafter, it remains fairly constant up to 2,000 cycles. After 2,000 cycles, the specific capacitance is still about 96.5% of the initial specific capacitance. Therefore, the CZ electrode shows high stability and retains its electrochemical capacitance property over 2,000 cycles.

EIS is further employed to monitor the electrochemical behavior of the electrodes. The resistance of a supercapacitor, namely equivalent series resistance or ESR, consists of electronic contributions and ionic contributions. Typical Nyquist impedance spectra recorded at a frequency range of 100 kHz to 10 mHz for CC and CZ are shown in Fig. 10. At very high frequencies, the intercept at the real axis is the ESR value. It can be seen that the ESR of CZ (0.7 Ω) is much lower than that of CC (1.3 Ω), indicating that the electric conductivity increases. The lower electronic resistance for CZ is probably attributable to more rapid mass transport within micropores of carbon due to the improved wettability of active material [31]. The imaginary part of the impedance spectra at low frequencies represents the capacitive behavior of the electrode and approaches a 90° vertical line in an ideal capacitor [20]. In the low-frequency region, the slope of CZ is steeper than that of CC, which suggests that the capacitive performance is better than that of CC. This is consistent with the above results of CV curves.

Figure 11 illustrates the equivalent circuit used to model the impedance response. Therein, in the high frequency, the equivalent circuit for CC and CZ electrodes involves the following elements: the solution resistance, R_s, the capacitance at the contact interface of carbon particals, C_C, which was expected in parallel with the contact resistance (R_c). In addition, in the low frequency region, a low-frequency capacitance (C_L) in parallel with a charge transfer resistance

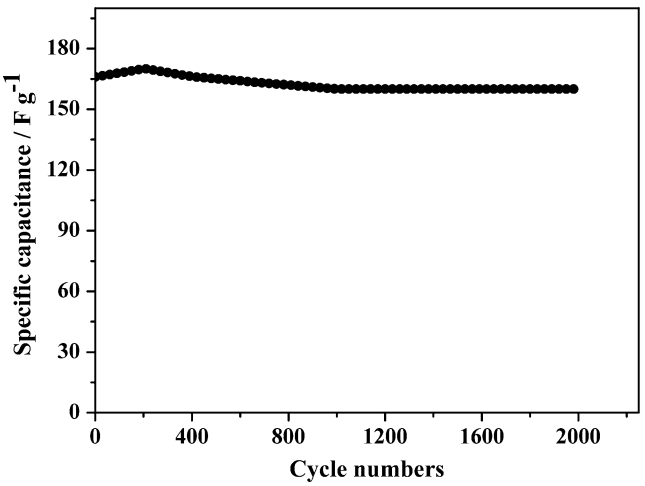

Fig. 9 Charge/discharge cycling stability of CZ at a current density of 500 mA g^{-1}. Specific capacitance calculated from discharge profiles of galvanostatic cycling curves measured in two-electrode cells

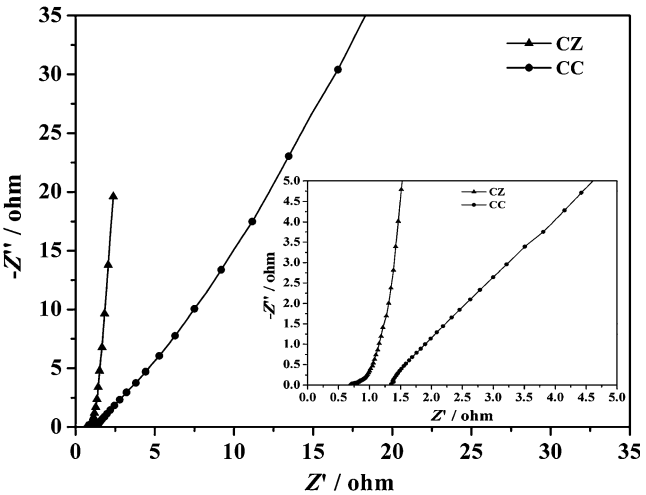

Fig. 10 Nyquist plot of the CC and CZ (*inset* enlarged high-frequency region of Nyquist plot)

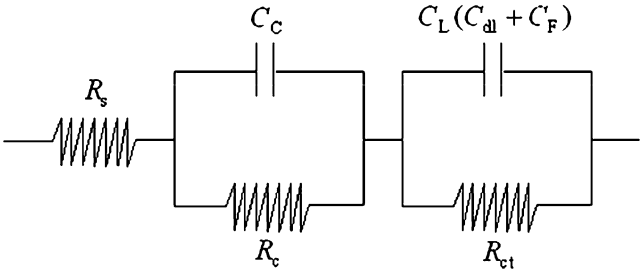

Fig. 11 Equivalent circuit for simulating the impedance spectra of the CC and CZ electrodes

(R_{ct}). C_L in the circuit model represents the combination of the double-layer capacitance (C_{dl}) and the pseudocapcacitance (C_F), though the mechanisms between these two (C_{dl} and C_F) are different. C_C and C_L are the constant phase elements associated with R_c and R_{ct}.

Conclusions

Activated carbon has been prepared from PANI by chemical activation using $ZnCl_2$ as an active reagent. Compared with the CC, CZ shows porous textures and remarkable enhancements in the specific surface area and volume of micropores. As the electrode materials for the application of supercapacitors, CZ exhibits better capacitive performance and has high specific capacitance of 174 $F g^{-1}$. Correlating the capacitive behavior with textural characteristics, the good electrochemical performance of the activated carbon is ascribed to high surface area (824 m^2 g^{-1}), well-developed micropores, low equivalent series resistance (0.7 Ω), and the presence of electrochemically active quinone oxygen groups and nitrogen functional groups.

Acknowledgments The authors are grateful for the project supported by Hunan Provincial Natural Science Foundation of China (07JJ6015).

References

1. Du QL, Zheng MB, Zhang LF, Wang YW, Chen JH, Xue LP, Dai WJ, Ji GB, Cao JM (2010) Electrochim Acta 55:3897–3903
2. Wen ZB, Qu QT, Gao Q, Zheng XW, Hu ZH, Wu YP, Liu YF, Wang XJ (2009) Electrochem Commun 11:715–718
3. Kalpana D, Cho SH, Lee SB, Lee YS, Misra R, Renganathand NG (2009) J Power Sources 190:587–591
4. Xia KS, Gao QM, Jiang JH, Hu J (2008) Carbon 46:1718–1726
5. Wang YQ, Yuan AB, Wang XL (2008) J Solid State Electrochem 12:1101–1107
6. Lin JH, Ko TH, Lin YH, Pan CK (2009) Energy Fuels 23:4668–4677
7. Juan Y, Qiang QK (2009) Environ Sci Technol 43:3385–3390
8. Pandolfo AG, Hollenkamp AF (2006) J Power Sources 157:11–27
9. Wang HQ, Zhong YL, Li QY, Yang JH, Dai QH (2008) J Phys Chem Solids 69:2420–2425
10. Rufford TE, Hulicova-Jurcakova D, Khosla K, Zhu ZH, Lu GQ (2010) J Power Sources 195:912–918
11. Jisha MR, Hwang YJ, Shin JS, Nahm KS, Kumard TP, Karthikeyand K, Dhanikaivelud N, Kalpanad D, Renganathand NG, Stephand AM (2009) Mater Chem Phys 115:33–39
12. Baçaoui A, Yaacoubi A, Dahbi A, Bennouna C, Luu RPT, Maldonado-Hodar FJ, Rivera-Utrilla J, Moreno-Castilla C (2001) Carbon 39:425–432
13. Zhang TY, Walawender WP, Fan LT, Fan M, Daugaard D, Brown RC (2004) Chem Eng J 105:53–59
14. Olivares-Marin M, Fernández-González C, Macías-García A, Gómez-Serrano V (2006) Appl Surf Sci 252:5967–5971
15. Zhang GQ, Zhang ST (2009) J Solid State Electrochem 13:887–893
16. Xing W, Huang CC, Zhuo SP, Yuan X, Wang GQ, Hulicova-Jurcakova D, Yan ZF, Lu GQ (2009) Carbon 47:1715–1722
17. Hsu LY, Teng H (2000) Fuel Process Technol 64:155–166
18. Nakagawa Y, Molina-Sabio M, Rodríguez-Reinoso F (2007) Microporous Mesoporous Mater 103:29–34
19. Guo YP, Rockstraw DA (2007) Microporous Mesoporous Mater 100:12–19
20. Li LM, Liu EH, Li J, Yang YJ, Shen HJ, Huang ZZ, Xiang XX, Li W (2010) J Power Sources 195:1516–1521
21. Horng YY, Lu YC, Hsu YK, Chen CC, Chen LC, Chen KH (2010) J Power Sources 195:4418–4422
22. Seredych M, Hulicova-Jurcakova D, Lu GQ, Bandosz TJ (2008) Carbon 46:1475–1488
23. Lota G, Grzyb B, Machnikowska H, Machnikowski J, Frackowiak E (2005) Chem Phys Lett 404:53–58
24. Lua AC, Yang T (2005) J Colloid Interface Sci 290:505–513
25. Nowicki P, Pietrzak R, Wachowska H (2010) Energy Fuels 24:1197–1206
26. Gu L, Zhang XW, Lei LC (2008) Ind Eng Chem Res 47:6809–6815
27. Figueiredo JL, Pereira MFR, Freitas MMA, Órfão JJM (1999) Carbon 37:1379–1389
28. Hulicova-Jurcakova D, Seredych M, Lu GQ, Bandosz TJ (2009) Adv Funct Mater 19:438–447
29. Jurewicz K, Babel K, Źiółkowski A, Wachowska H (2003) Electrochim Acta 48:1491–1498
30. Hulicova-Jurcakova D, Seredych M, Jin YG, Lu GQ, Bandosz TJ (2010) Carbon 48:1767–1778
31. Fang BZ, Binder L (2006) J Phys Chem B 110:7877–7882